









# Synthesis of magnetic nanostructures in different carbon matrices and post annealing with oxygen, nitrogen and argon

Cite as: AIP Advances 15, 035226 (2025); doi: 10.1063/9.0000939

Submitted: 12 November 2024 • Accepted: 14 February 2025 •

Published Online: 17 March 2025



Vicente Pena Perez,  Cristian Reynaga Gonzalez,  Erick Villegas, Jonah Baughman,  Lorena Aguirre,  Franco Iglesias,  Armond Khodagulyan,  Oscar O. Bernal,  and Armen N. Kocharian<sup>a)</sup> 

## AFFILIATIONS

Physics Department, California State University, Los Angeles, California 90032, USA

**Note:** This paper was presented at the 16th Joint MMM-Intermag Conference.

<sup>a)</sup> Author to whom correspondence should be addressed: [akochar@calstatela.edu](mailto:akochar@calstatela.edu)

## ABSTRACT

This study explores the innovative use of carbon matrices in the synthesis of magnetic nanographite, layered graphene stacks and graphene coated magnetic nanoparticles, with a focus on their morphological, structural, and magnetic properties. To obtain a deeper insight into the influences of impurities in the graphene matrices on the magnetic properties of synthesized by pyrolysis, the two different metal free modifications of porphyrin such as tetraphenyl porphyrin (TPP) and tetra(4-carboxyphenyl) porphyrin (TCPP) with oxygen content (radical) were synthesized by subsequential post annealing with oxygen, argon and nitrogen, to characterize and investigate the role of oxygen and nitrogen content in graphene environment. The research highlights the significance of porphyrin and phthalocyanine metal free precursors and their metal counterparts for use as carbon matrices, examining their unique characteristics and applications in nanoparticle synthesis by sequential annealing. For example, the magnetization figure below for TPP indicates that the samples are diamagnetic at relatively high temperatures and large magnetic fields. Annealing at 150 °C for 180 min, specifically, for oxygen, it increases paramagnetic behavior and saturation. As for nitrogen, it increases coercivity. Employing advanced characterization techniques such as powder x-ray diffraction (PXRD), we analyzed the graphitization and porosity effects and layer sizes of nanographite and their impact on magnetic properties. A novel algorithm, integrating node extraction and 2D Gaussian mapping, is developed to enhance the accuracy of morphological analysis. Our findings reveal the critical role of graphene, and role of oxygen and nitrogen impurities in influencing the magnetic behavior of metal free carbon matrices and embedded nanoparticles, providing valuable insights into the design and development of advanced magnetic nanomaterials.

© 2025 Author(s). All article content, except where otherwise noted, is licensed under a Creative Commons Attribution-NonCommercial-NoDerivs 4.0 International (CC BY-NC-ND) license (<https://creativecommons.org/licenses/by-nc-nd/4.0/>). <https://doi.org/10.1063/9.0000939>

## I. INTRODUCTION

There is great interest in the possible existence of ferromagnetism well above room temperature in non-magnetic bulk materials which have no transition or rare earth metal components. Ferromagnetism with high Curie temperature  $T_C$ , well above room temperature, and very small saturation moments have been reported in various boron and carbon systems with itinerant electrons occupying a narrow impurity band in highly oriented pyrolytic graphite.<sup>1</sup> Such high-temperature intrinsic ferromagnetism, recently reported

in carbon systems such as graphite nanoclusters with the stacking graphene layers in graphene microspheres,<sup>2–4</sup> originated from localized electron states at lattice imperfections such as point defects, zigzag edges, nitrogen impurities, and carbon vacancies.<sup>5</sup> Finite size ribbons display remarkably sharp peaks in the density states at the Fermi level which do not originate from the infinite graphite lattice.<sup>6</sup> Induced ferromagnetic exchange in non-magnetic materials mediated via electron or hole doping with non-transition metals is primarily attributed to  $s$  and  $p$  orbitals.<sup>7,8</sup> An effective exchange interaction in diluted magnetic semiconductors (DMS) can be described by

various factors, e.g., including hybridization of electron or hole states with the valency and conducting bands, total intra-atomic exchange, including intra-band electron and Coulomb interaction in contrast to traditional ferromagnetism of 3d/4f electrons explaining the stability of ferromagnetism vs. antiferromagnetism in chalcogenides within a perturbation approach.<sup>9–11</sup>

Below we present the results of investigations of structural and magnetic properties in multilayer graphene nanoclusters (nanographite) and their changes due to activated carbonization, amorphization, and graphitization under pyrolysis, as well as the influence of adsorbed oxygen, nitrogen, and argon molecules under processes of annealing. For understanding and governing defect-induced ferromagnetism with high Curie temperature  $T_c$ , well above room temperature, magnetic and electronic properties of nanoparticles have been of significant interest to the scientific community, with extensive research conducted through texture analysis, lattice fringe imaging, and micro- and nano-structural analysis, as demonstrated in the analysis of coal char using High-Resolution Transmission Electron Microscopy (HRTEM) by Sharma, Kyotani, and Tomita.<sup>12,13</sup>

The synthesis of metal nanoparticles (Fe, Ni, Co) necessitates a comprehensive understanding of the metal-free matrices that serve as foundational precursors. These matrices not only determine the fundamental structure but also influence the resultant properties of the synthesized nanoparticles. This chapter provides an overview of three critical precursors: Phthalocyanine, TPP-porphyrin, and TCPP-porphyrin, each exhibiting unique characteristics that make them ideal candidates for metal nanoparticle synthesis. Phthalocyanine ( $C_{32}H_{18}N_8$ ), a macrocyclic compound with remarkable electronic and optical properties due to its extensive  $\pi$ -conjugation, is widely used in dyeing, organic semiconductors, and photovoltaic devices because of its stable chemical properties. In nanoparticle synthesis, Pc serves as a stable matrix that facilitates the control of size and distribution of metal nanoparticles, with its  $\pi$ -conjugation enabling efficient electron transfer, thereby influencing the electronic properties of the nanoparticles.

TPP ( $C_{44}H_{30}N_4$ ), closely resembling natural porphyrin, plays a crucial role in the study of biomimetic systems by modeling the active sites of metalloproteins. It is pivotal in research related to photodynamic therapy and solar energy conversion. The synthetic flexibility of TPP allows for the introduction of various functional groups, enhancing its affinity for metal ions, and thus controlling the formation and stabilization of metal nanoparticles. TCPP porphyrin ( $C_{48}H_{30}N_4O_8$ ), a porphyrin derivative, boasts enhanced solubility and reactivity due to its carboxyphenyl groups, with applications ranging from catalysis to sensor development and photodynamic therapy. The carboxylic groups in TCPP not only improve solubility but also provide sites for subsequent functionalization, influencing the nanoparticle surface chemistry and introducing new properties to the metallic centers.

The choice of the metal-free matrix is a critical step in the synthesis of metal nanoparticles. The properties of Pc, TPP, and TCPP, such as their  $\pi$ -conjugation systems and functional groups, offer a versatile platform for tailoring the characteristics of metal nanoparticles. Distinct variations in magnetic properties arise from the interaction of metal ions with Pc, TPP, and TCPP. These variations are primarily influenced by the structural characteristics and electronic environments of each macrocycle.<sup>2,14</sup> Pc, with its symmet-

ric, nitrogen-rich core, forms highly stable and evenly distributed complexes with metals such as Cu and Fe, exhibiting paramagnetic properties depending on the oxidation state and coordination geometry of the metal ion. In contrast, TPP, with its larger, more flexible structure due to phenyl substituents at the meso positions, can accommodate a variety of metal ions, leading to diverse magnetic behaviors, including diamagnetism in its metal free state and varying degrees of paramagnetism when complexed with metals like Mn or Co.

TCPP stands out due to its additional carboxyphenyl groups, which enhance solubility and interaction with metal ions, facilitating the attachment of multiple metal centers. This can lead to intricate magnetic interactions such as antiferromagnetic or ferromagnetic coupling between adjacent metal ions, depending on the method of nanoparticle synthesis and the spatial arrangement of the TCPP ligands around the metal centers. Thus, the choice of a metal-free matrix and its specific interaction with metal ions crucially dictates the magnetic characteristics of the synthesized nanoparticles, offering tailored functionalities for advanced material applications.<sup>14–17</sup>

## II. EXPERIMENT

The process begins with the precise measurement of the precursor masses, typically between 100–200 g. These samples are then carefully sealed under vacuum using an oxygen-acetylene torch to ensure an airtight environment, followed by heat treatment at controlled temperatures ranging from 250 to 900 °C. The duration of this heat treatment varies between 10 and 180 min, depending on the specific requirements for nanoparticle formation and growth. After pyrolysis, the samples undergo a deagglomeration process, which includes grinding with a pestle and mortar and ultrasonic dispersion in isopropyl alcohol (IPA) for at least 60 min. This step ensures a uniform particle size distribution, crucial for subsequent analyses. Following ultrasonic treatment, the samples are centrifuged and subjected to magnetic separation to assess their initial magnetization. The samples are then dried under vacuum in a desiccator overnight. Optional annealing is conducted in a controlled environment using nitrogen, oxygen, or argon gases at 150 °C for 180 min. This process further refines the material's properties by influencing the interaction of the gas with the sample. Characterization of the synthesized matrices is performed using several advanced techniques. The Physical Property Measurement System (PPMS by Quantum Design) is used to measure the magnetic response, providing hysteresis loops that are crucial for understanding the material's magnetic properties as shown in Table I. Powder x-ray Diffraction (PXRD) analysis is carried out to determine crystallinity and nanoparticle sizes, with data collected over a range of 10° to 90° in two theta  $2\theta$ . Scanning Electron Microscopy (SEM) coupled with Energy Dispersive Spectroscopy (EDS) and Channeling Backscatter Spectroscopy (CBS) is employed for detailed elemental analysis and to observe the morphology and porosity of the samples. Transmission Electron Microscopy (TEM) can be used to gain further insights into the layer composition, edge morphology, and porosity maps, offering a comprehensive understanding of the material structure. Magnetization consists of three contributions: ferromagnetic, paramagnetic, and diamagnetic which are temperature independent.<sup>2</sup>

TABLE I. Summary of magnetic properties for Pc, TPP, TCPP, and TCPP:TPP under various conditions.

Precursor	Temperature (K)	Ms (emu/g)	Mr (emu/g)	Hc (Oe)
Pc 900 °C 10 min non-annealing	300	0.023	0.001 5	99.24
Pc 900 °C 10 min + O <sub>2</sub> annealing	10	0.041	0.001 9	199.34
TPP 900 °C 10 min non-annealing	10	0.005 5	0.000 66	254.13
TPP 900 °C 10 min + O <sub>2</sub> annealing	300	0.007 5	0.000 13	177.16
TCPP 900 °C 10 min non-annealing	20	0.000 538	0.000 858	1917.56
TCPP 900 °C 10 min + N <sub>2</sub> annealing	300	0.013 3	0.000 112	698.13
TCPP:TPP 50%–50%, 900 °C 10 min non-annealing	300	0.000 47	0.000 25	210.17
TCPP:TPP 50%–50%, 900 °C 10 min non-annealing	10	0.017	0.000 53	167.37

III. RESULTS

A. Phthalocyanine (Pc)

Phthalocyanine (Pc) demonstrated distinct magnetic behaviors under varying conditions. At 300 K, the Pc samples in Fig. 1 exhibited a clear diamagnetic behavior, which was further influenced by nitrogen annealing, leading to a decrease in saturation magnetization. This reduction is likely due to the re-incorporation of nitrogen vacancies during the annealing process. At 10 K, the Pc samples showed paramagnetic behavior, with nitrogen annealing diminishing the magnetic saturation. The optimal conditions for maximizing the  $\frac{M_r}{M_s}$  ratio were identified as pyrolysis at 900 °C for 10 min at 300 K, yielding a ratio of 0.067. In contrast, the least favorable conditions were with oxygen annealing at 10 K, resulting in a ratio of 0.046.

B. Tetraphenylporphyrin (TPP)

Tetraphenylporphyrin (TPP), in Figs. 2 and 3, exhibited the most pronounced diamagnetic behavior among the studied precursors. Oxygen annealing significantly influenced the magnetic properties, decreasing diamagnetism and enhancing paramagnetism at 300 K. At 10 K, the TPP samples displayed superparamagnetic behavior, with oxygen annealing further enhancing this response. The optimal conditions for maximizing the  $\frac{M_r}{M_s}$  ratio were achieved with pyrolysis at 900 °C for 10 min, followed by measurements at 10 K, yielding a ratio of 0.11. The least favorable conditions involved oxygen annealing at 300 K, with a ratio of 0.0081. The  $M(T)$  curve for TPP, Fig. 4, at  $H = 60\text{kOe}$  shows a steady decrease in magnetization with increasing temperature, consistent with a paramagnetic response. The lack of thermal hysteresis indicates the

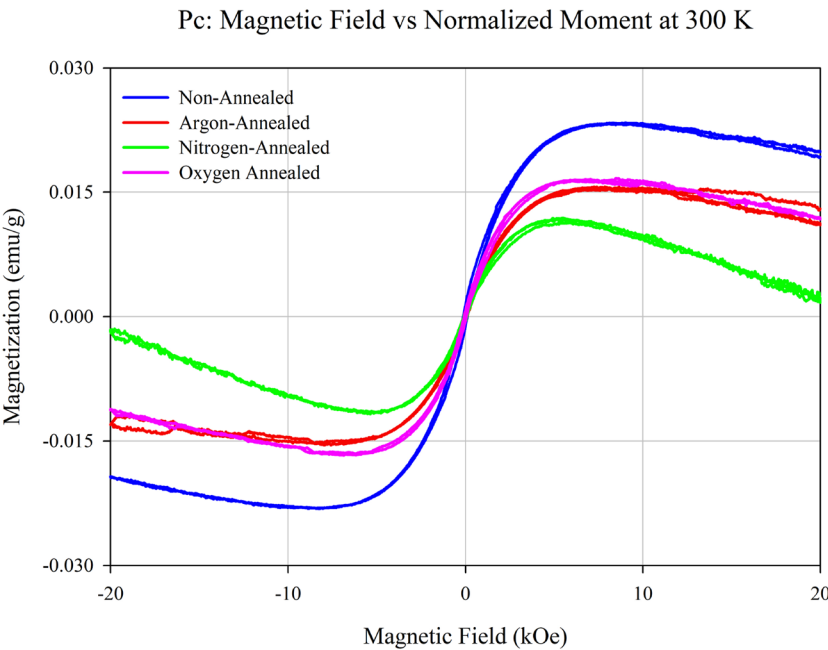
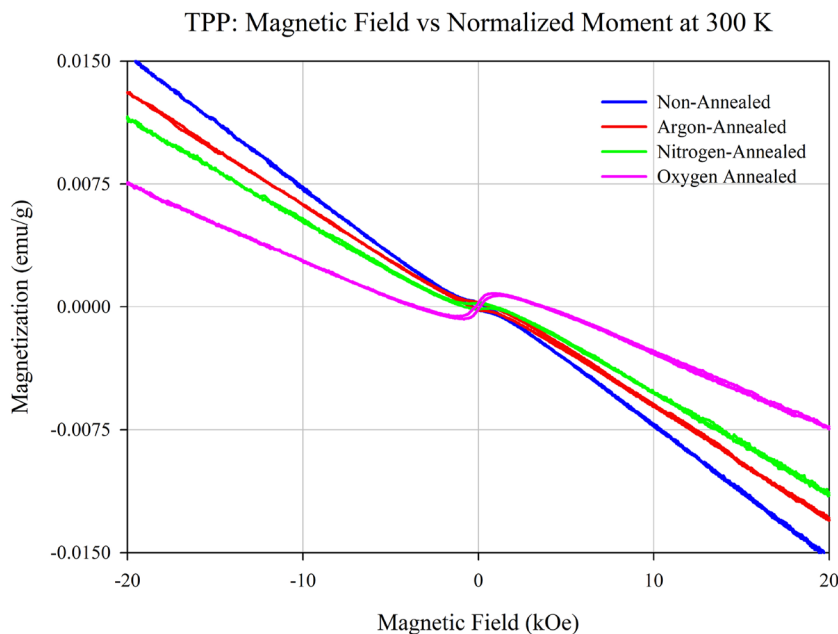
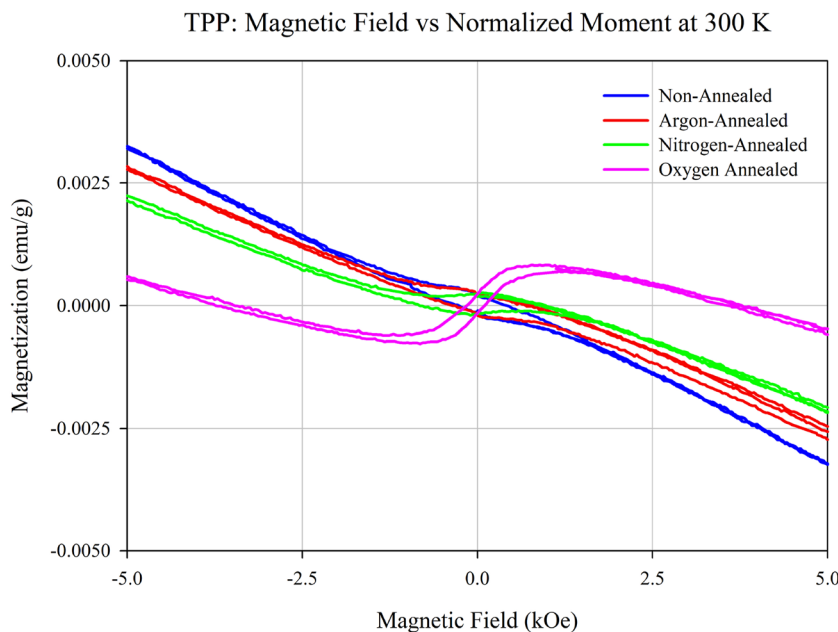


FIG. 1. All hysteresis loops for Pc samples with pyrolysis at 900 °C for 10 min, measuring magnetic moment at 300 K with a maximum applied field of  $H = 20\text{kOe}$ . It gradually increases in saturation while showing paramagnetism, then it decreases at larger magnetic fields showing diamagnetism.



**FIG. 2.** All hysteresis loops for TPP samples with pyrolysis at 900 °C for 10 min, measuring magnetic moment at 300 K with a maximum applied field of  $H = 20$  kOe. Samples show saturation a small magnetic field, then become diamagnetic at large magnetic fields.



**FIG. 3.** Zoom into the ferromagnetic part of the hysteresis loop for TPP.

absence of significant structural rearrangements or phase transitions over this temperature range. TPP maintains positive magnetization at temperatures lower than 10 K. Then, it becomes negative for higher temperatures indicates a weaker paramagnetic contribution from localized magnetic moments or structural defects compared to TCPP. Note, the starting of these hysteresis loops were removed on the zoomed versions to distinguish loops.

### C. Tetrakis(4-carboxyphenyl) porphyrin (TCPP)

Figures 5 and 6 display TCPP slightly less diamagnetic behavior than TPP. The magnetic properties of TCPP were sensitive to temperature changes, with the samples showing layer-wise temperature dependence. Oxygen annealing improved stability and enhanced magnetic saturation, especially at lower temperatures. The optimal conditions for TCPP were pyrolysis at 900 °C for 10 min, with measurements at 20 K yielding an  $\frac{M_r}{M_s}$  ratio of 1.59. Nitrogen annealing

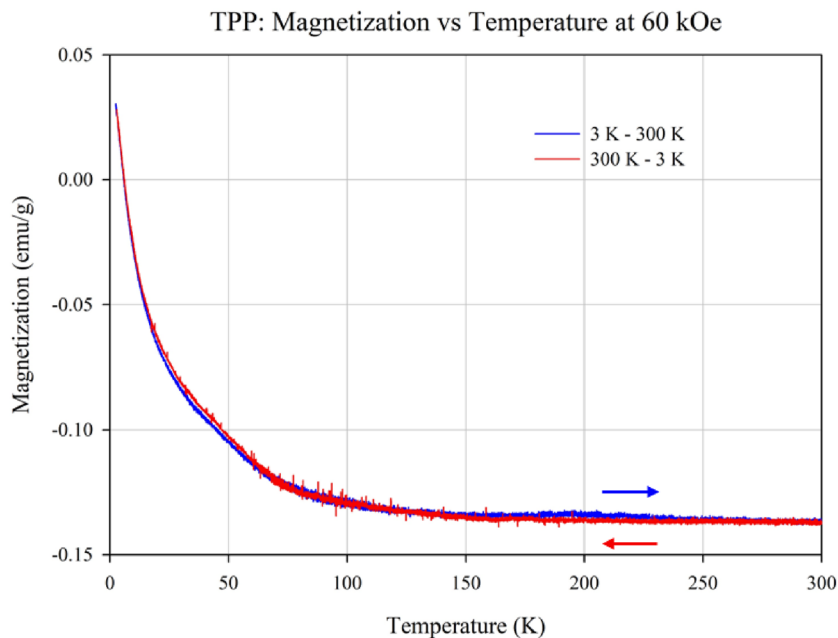


**FIG. 4.** Temperature dependence of magnetization  $M(T)$  for TPP under constant magnetic field. The blue curve represents heating, while the red curve represents cooling. The steady decrease in magnetization with temperature suggests dominant paramagnetic contributions, consistent with localized defect states. At large temperature the sample displays temperature independent diamagnetism. Magnetic susceptibility was found to be  $-2.16 \times 10^{-6} \text{ emu g}^{-1} \text{ Oe}^{-1}$ .

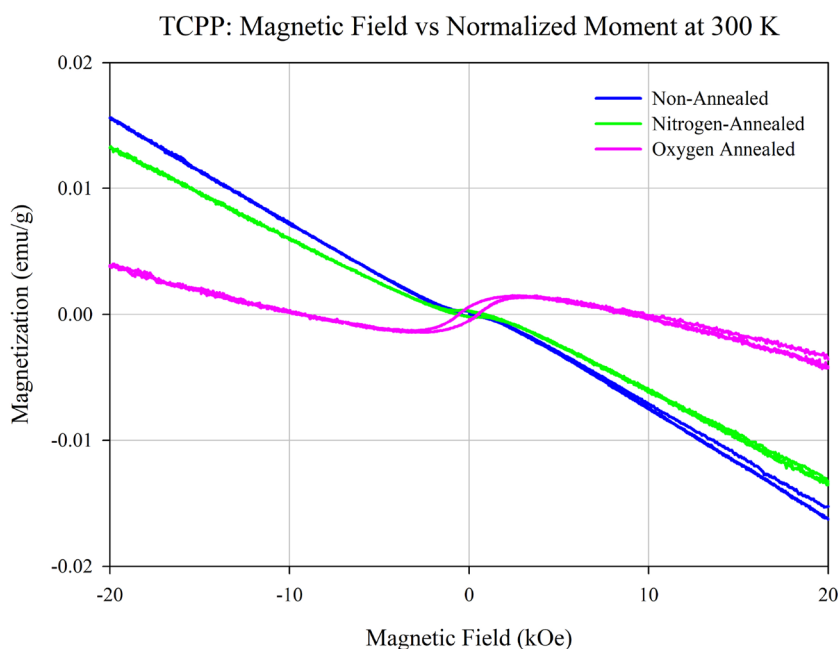


**FIG. 5.** All hysteresis loops for TCPP samples with pyrolysis at  $900^\circ\text{C}$  for 10 min, measuring magnetic moment at 300 K with a maximum applied field of  $H = 20 \text{ kOe}$ . Annealing conditions for all were at  $150^\circ\text{C}$  for 180 min. Inset shows the ferromagnetic region of the loops.

at 300 K resulted in the least favorable conditions, with a ratio of 0.0084. The  $M(T)$  curve for TCPP, Fig. 7, at  $H = 60 \text{ kOe}$  shows a steady decrease in the magnetization just as TPP; however, note that it drops below  $0.00 \text{ emu/g}$  at a higher temperature compared to TPP which indicates that the diamagnetic contribution outweighs any paramagnetic or ferromagnetic components at higher temperatures. Diamagnetic behavior arises from the orbital motion of electrons,

which generates a weak, temperature-dependent magnetic response opposing the applied field. This suggests that TCPP has many more localized magnetic moments (paramagnetic centers) or edge states capable of contributing to positive magnetization compared to TPP. Note that the argon annealing results are not included due to the floor noise of the vibrating sample magnetometer (VSM) floor noise getting close to the actual magnetization measured by the PPMS.

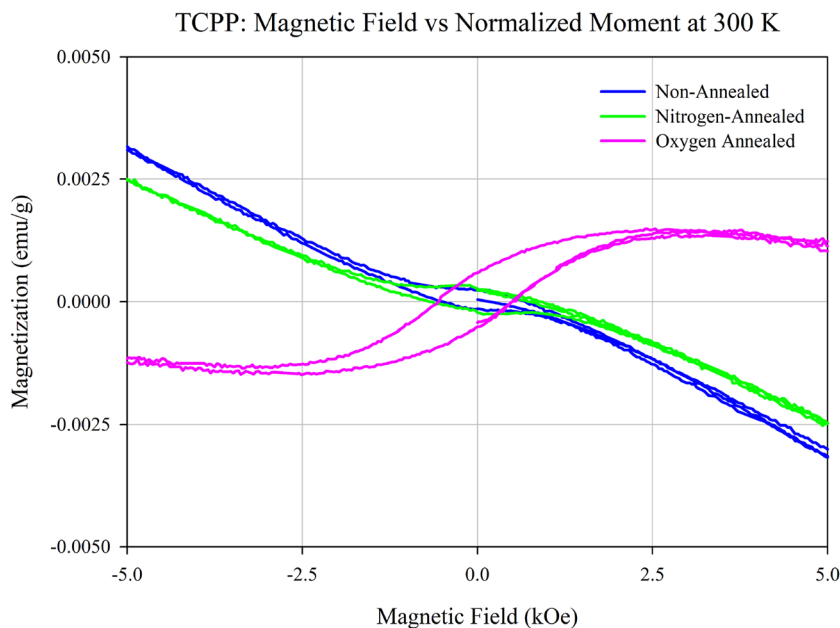


FIG. 6. Zoom into the ferromagnetic part of the hysteresis loop for TCPP.

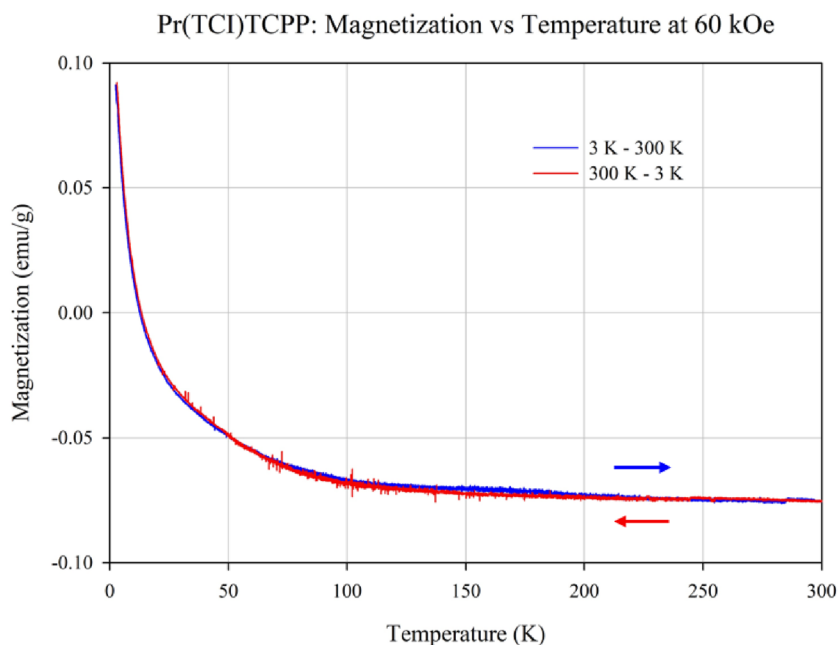


FIG. 7. Temperature-dependent magnetization  $M(T)$  of TCPP at 60 kOe. The stronger diamagnetic behavior compared to TPP reflects reduced graphitic edge states and higher oxygen content in the TCPP matrix. Magnetic susceptibility was found to be  $-1.25 \times 10^{-6} \text{ emu g}^{-1} \text{ Oe}^{-1}$ .

#### D. TCPP:TPP concentration variations

The study also explored various concentrations of TCPP and TPP to identify the most stable mixture. As shown in Fig. 8, 75% TCPP with 25% TPP blend was the most stable at 300 K, while the 25% TCPP with 75% TPP blend showed the best magnetic saturation at 10 K. Oxygen annealing across all concentrations maintained diamagnetic behavior. The optimal  $\frac{M_z}{M_s}$  ratio was observed in the 50% TCPP and 50% TPP mixture at 300 K, with a ratio of 0.54, while the

least favorable was the same blend ratio at 10 K, yielding a ratio of 0.000 53.

#### E. PXRD for carbon matrices Pc, TCPP, and TPP

Given the complexity of the measurements, this section focuses on qualitative analyses of the Powder x-ray Diffraction (PXRD) patterns for the carbon matrices Pc, TCPP, and TPP. This approach allows us to observe fundamental structural differences without



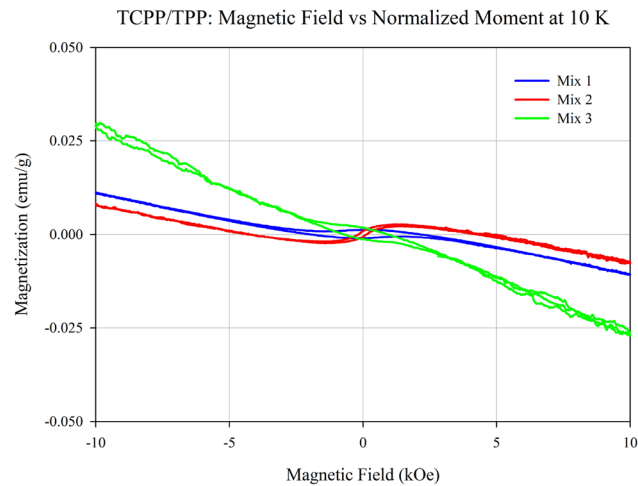


**FIG. 8.** Hysteresis loops for different concentration of TCPP and TPP with pyrolysis at 900 °C for 10 min and oxygen annealed at 150 °C for 180 min, measuring magnetic moment at 10 K with a maximum applied field of  $H = 20\text{kOe}$ . Inset shows the ferromagnetic region of the loops. Mix 1 represents 25% TCPP and 75% TPP. Mix 2 represents 50% TCPP and 50% TPP. Finally, Mix 3 represents 75% TCPP and 25% TPP.

delving into quantitative crystallite size calculations. Such results are listed in Table II. Figures 9 and 10 shows that the most prominent difference in the diffraction patterns is the absence of an initial intensity jump in TCPP, which is present in the other matrices; however, the small peak at  $11^\circ$  shows that TCPP indeed contains oxidizing layers (oxygen layers) in the matrix. This feature can be attributed to the higher oxygen content in TCPP due to its carboxyphenyl groups, which influence the lattice structure and

**TABLE II.** Elemental composition of various carbon matrices and their mixtures (900 °C–10 min). All samples were measured after pyrolysis free of annealing.

Matrix	Element	Weight %
TCPP	C	97.4
	Si	2.5
TPP	C	97.5
	Si	1.4
Pc	C	99.5
	Si	0.3
50% TCPP/50% TPP	C	93.1
	O	6.9
25% TCPP/75% TPP	C	69.9
	O	15.9
	N	9.3
	Si	4.9
75% TCPP/25% TPP	C	97.6
	Si	2.4

reduce the degree of structural ordering at certain diffraction angles. This structural difference correlates with the distinct magnetization behavior observed in TCPP, where the diamagnetic response dominates at higher temperatures, as demonstrated in the  $M(T)$  measurements. The oxygen within the lattice appears to suppress edge-state or defect-related magnetic contributions, leading to a more pronounced structural order compared to TPP. The recovery observed in the annealed TCPP samples suggests that annealing facilitates some degree of recrystallization or reordering within the TCPP matrix, potentially by affecting oxygen-related defects or rearranging the lattice structure. These changes in structural dynamics are consistent with the enhanced magnetization stability observed in annealed samples and are crucial for understanding the interplay between thermal treatment and magnetic properties. The qualitative PXRD analysis has provided valuable insights into the structural characteristics of Pc, TCPP, and TPP matrices, particularly in linking elemental composition and thermal treatment to diffraction patterns and magnetic behavior. Further quantitative studies, such as detailed crystallite size calculations and high-resolution structural analysis, would be necessary to precisely define the crystallographic properties and their impact on the observed magnetic trends.

F. Morphological analysis algorithm

To enhance the accuracy and reproducibility of morphological analysis, we implemented a novel algorithm based on previous approaches, such as those described by Sharma *et al.* This algorithm combines 2D Gaussian filtering with advanced junction detection and categorization to extract key features from SEM images, including microsphere size, density, and porosity. Our improved version of the algorithm begins with node extraction and skeletonization of the SEM images, followed by advanced reconnection procedures and junction categorization. This process allows for the precise identification of structural elements, such as Y, T, X, and L junctions, as well as features specific to materials like hematite and magnetite. These detailed classifications provide quantitative insights into the structural differences among the carbon matrices (Pc, TPP, and TCPP), supporting our observations of their distinct morphological and magnetic behaviors.

G. SEM and EDS for carbon matrices

SEM images (Fig. 11) reveal distinct morphological differences across the carbon matrices. In (Fig. 12) Pc exhibits smaller, denser microspheres, while TPP shows larger ones, and TCPP shows almost none. These structural variations correlate with the magnetic properties, where smaller or absent microspheres in TCPP and TPP are linked to better ferromagnetic responses, while larger microspheres in TPP are associated with paramagnetic behavior. EDS analysis shows that all matrices are predominantly composed of carbon, with minor traces of silicon, likely from the quartz tubes used in pyrolysis. The SEM and EDS results underscore the impact of microstructure on magnetic properties, providing valuable insights for material optimization.

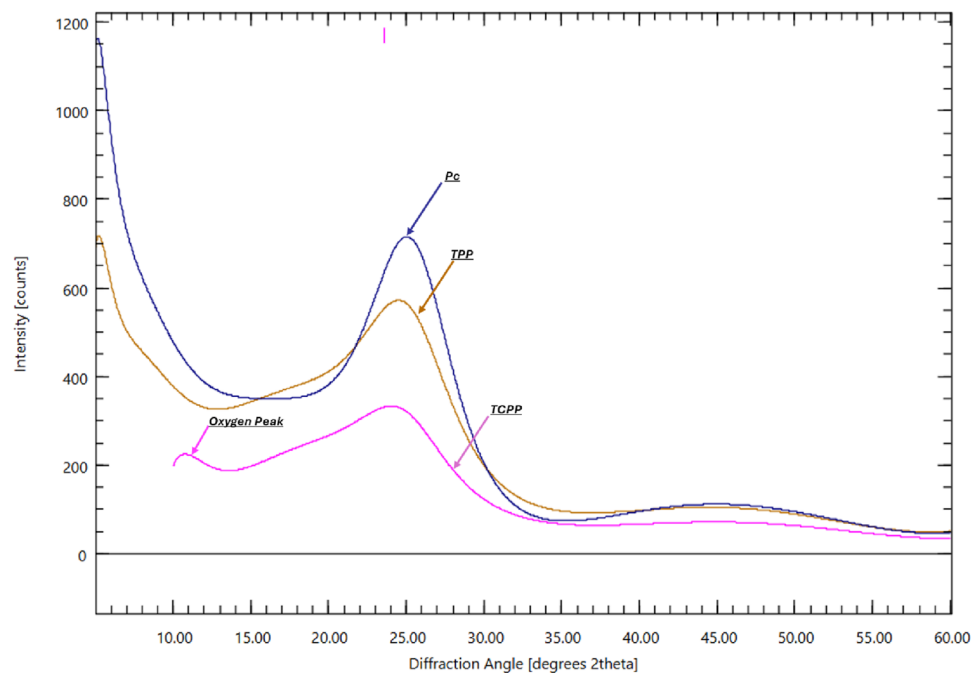


**FIG. 9.** PXRD measurements for all carbon matrices: Pc, TCPP, and TPP. They were pyrolyzed at 900 °C for 10 min.

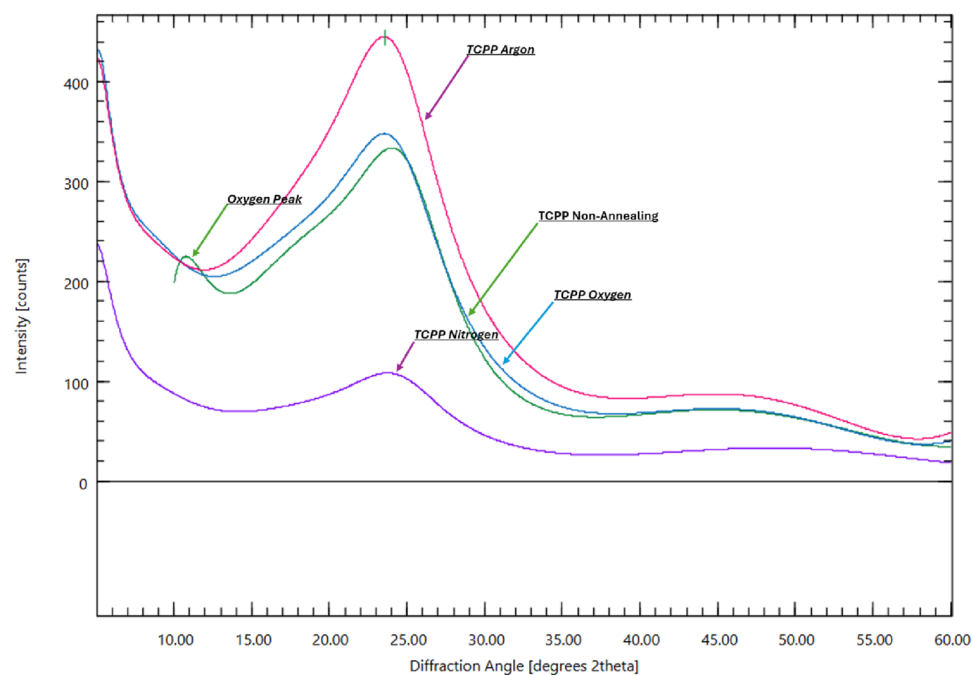


**FIG. 10.** PXRD measurements for TCPP matrices. They were pyrolyzed at 900 °C for 10 min. Also, annealed plots are shown.



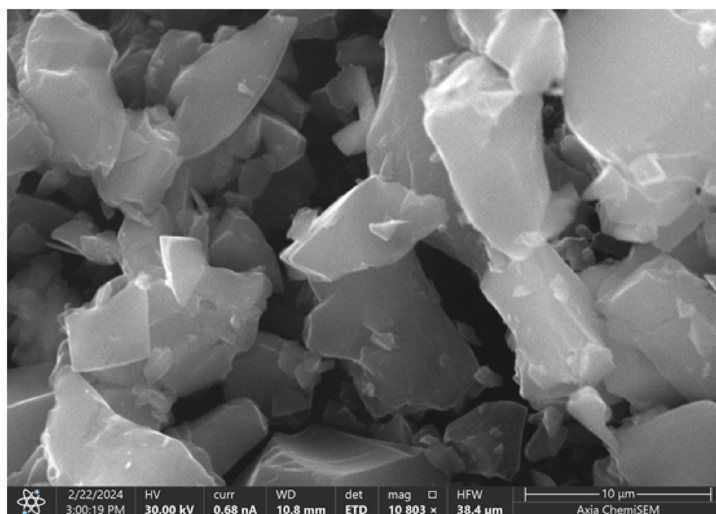


FIG. 11. SEM image for carbon matrices: TCPP.

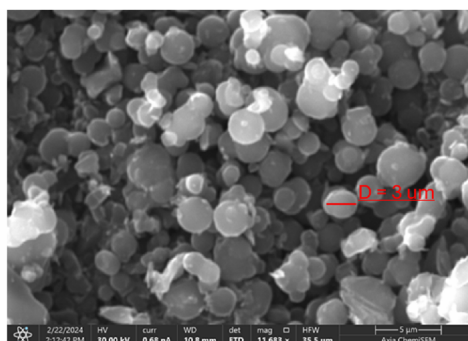
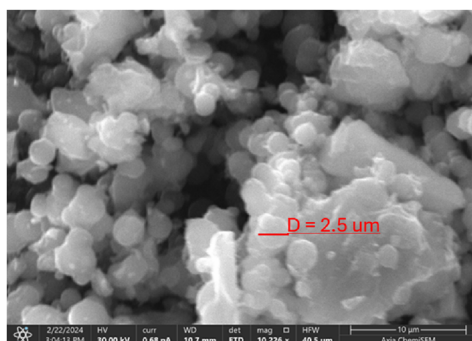


FIG. 12. SEM images for carbon matrices: Pc and TPP.

#### IV. CONCLUSION

SEM analysis revealed distinctive morphological variations among the carbon matrices. Phthalocyanine (Pc) displayed smaller, denser microspheres, Tetraphenylporphyrin (TPP) had larger microspheres, and Tetrakis(4-carboxyphenyl)porphyrin (TCPP) exhibited almost none. These differences correlate with magnetic behaviors: TCPP's sparse microspheres enhanced ferromagnetic responses, while TPP's larger microspheres aligned with paramagnetic tendencies. EDS analysis confirmed that carbon is the primary element in all matrices, with trace silicon, likely from quartz tubes used in pyrolysis. Pc showed distinct magnetic properties across varying conditions; at 300 K, it was diamagnetic, while nitrogen annealing decreased saturation magnetization, possibly due to nitrogen vacancy reincorporation. The  $M(T)$  measurements provided further insights into the magnetic properties of TPP and TCPP. TPP maintained positive magnetization throughout the temperature range, reflecting strong paramagnetic contributions from localized edge states and defects. In contrast, TCPP exhibited a transition to negative magnetization at higher temperatures, indicating a dominant diamagnetic response due to its higher oxygen content and reduced defect density. These trends highlight the interplay between structural features, such as oxygen content and graphitic edge states, and magnetic behavior. PXRD analysis supported these findings, revealing that TCPP's higher oxygen

content reduced structural ordering and suppressed defect-driven magnetic contributions, while annealing facilitated partial recrystallization and lattice reordering. This study highlights how structural characteristics influence magnetic behavior, offering insights for optimizing materials for specific magnetic properties. Our findings are an important step toward bringing together chemical and physical aspects of activated carbon, different conditions of pyrolysis, role of graphene edges, nitrogen and oxygen impurities, and effects of annealing that may have strong implications for the research field of graphene-based nanoscale systems. The role of porosity in these nanostructures remains an intriguing aspect that could significantly influence both magnetic behavior and material functionality. In future work, we aim to investigate the effects of porosity on magnetic properties, as well as how it may interact with layer structuring and graphitization to impact overall performance. This line of research will provide a more comprehensive understanding of the material's potential in various applications.

#### ACKNOWLEDGMENTS

This work is supported by grants from the American National Science Foundation, Grants Nos. HRD-1547723 and HRD-2112554, as well as the National Institute of Health, Grant No. T34-GM08228.

## AUTHOR DECLARATIONS

## Conflict of Interest

The authors have no conflicts to disclose.

## Author Contributions

**Vicente Pena Perez:** Conceptualization (equal); Data curation (lead); Formal analysis (equal); Funding acquisition (equal); Investigation (equal); Methodology (equal); Project administration (equal); Resources (equal); Software (lead); Supervision (equal); Validation (supporting); Visualization (equal); Writing – original draft (equal); Writing – review & editing (equal). **Cristian Reynaga Gonzalez:** Data curation (equal); Formal analysis (equal); Funding acquisition (equal); Investigation (equal); Methodology (equal); Resources (equal). **Erick Villegas:** Resources (equal); Software (equal). **Jonah Baughman:** Formal analysis (equal); Investigation (equal); Methodology (equal); Project administration (equal); Resources (equal). **Lorena Aguirre:** Investigation (equal); Methodology (equal); Resources (equal); Software (equal). **Franco Iglesias:** Formal analysis (equal); Investigation (equal); Methodology (equal); Resources (equal); Software (equal). **Armond Khodagulyan:** Conceptualization (equal); Formal analysis (equal); Methodology (equal); Project administration (equal); Resources (equal); Supervision (equal); Visualization (equal); Writing – review & editing (equal). **Oscar O. Bernal:** Formal analysis (equal); Investigation (equal); Methodology (equal); Project administration (equal); Resources (equal); Software (equal). **Armen N. Kocharian:** Conceptualization (equal); Data curation (equal); Formal analysis (equal); Funding acquisition (equal); Investigation (equal); Methodology (equal); Project administration (equal); Resources (equal).

## DATA AVAILABILITY

The data that support the findings of this study are available from the corresponding author upon reasonable request.

## REFERENCES

- <sup>1</sup>J. Červenka, M. I. Katsnelson, and C. F. J. Flipse, “Room-temperature ferromagnetism in graphite driven by two-dimensional networks of point defects,” *Nat. Phys.* **5**, 840–844 (2009).
- <sup>2</sup>A. Manukyan, H. Gyulasyan, A. Kocharian, P. Oyala, R. Chumakov, M. Avramenko, C. Sanchez, O. O. Bernal, L. Bugaev, and E. Sharoyan, “Structure and magnetism of few-layer nanographene clusters in carbon microspheres,” *J. Phys. Chem. C* **126**, 493–504 (2022).
- <sup>3</sup>M. Koshino and T. Ando, “Diamagnetic response of graphene multilayers,” *Physica E* **40**, 1014–1016 (2008).
- <sup>4</sup>F. Lin, Z. Zhu, X. Zhou, W. Qiu, C. Niu, J. Hu, K. Dahal, Y. Wang, Z. Zhao, Z. Ren, D. Litvinov, Z. Liu, Z. M. Wang, and J. Bao, “Orientation control of graphene flakes by magnetic field: Broad device applications of macroscopically aligned graphene,” *Adv. Mater.* **29**, 1604453 (2017).
- <sup>5</sup>D. M. Edwards and M. I. Katsnelson, “High-temperature ferromagnetism of sp electrons in narrow impurity bands: Application to CaB<sub>6</sub>,” *J. Phys.: Condens. Matter* **18**, 7209 (2006).
- <sup>6</sup>M. Fujita, K. Wakabayashi, K. Nakada, and K. Kusakabe, “Peculiar localized state at zigzag graphite edge,” *J. Phys. Soc. Jpn.* **65**, 1920 (1996).
- <sup>7</sup>R. Skomski, J. Zhou, J. Zhang, and D. J. Sellmyer, “Indirect exchange in dilute magnetic semiconductors,” *J. Appl. Phys.* **99**, 08D504 (2006).
- <sup>8</sup>M. E. Potter, L. N. Riley, A. E. Oakley, P. M. Mhembe, J. Callison, and R. Raja, “The influence of porosity on nanoparticle formation in hierarchical aluminophosphates,” *Beilstein J. Nanotechnol.* **10**, 1952–1957 (2019).
- <sup>9</sup>A. N. Kocharyan and P. S. Ovnanyan, “Exchange interaction mechanisms in magnetic semiconductors,” *Sov. Phys. JETP* **47**, 620–628 (1978).
- <sup>10</sup>A. N. Kocharyan and D. I. Khomskii, “Exchange interaction in magnetic semiconductors,” *Sov. Phys. Solid State* **17**, 290–291 (1975).
- <sup>11</sup>A. N. Kocharyan and P. S. Ovnanyan, “Electron structure and mechanisms of indirect exchange in doped semiconductors,” *Sov. Phys. Solid State* **21**, 997–999 (1979).
- <sup>12</sup>A. Sharma, T. Kyotani, and A. Tomita, “A new quantitative approach for microstructural analysis of coal char using HRTEM images,” *Fuel* **78**, 1203–1212 (1999).
- <sup>13</sup>J. C. Joubert, D. N. Wilke, and P. Pizette, “Fourier image analysis of multi-phase interfaces to quantify primary atomization,” *Math. Comput. Appl.* **28**, 55 (2023).
- <sup>14</sup>B. Chilukuri, U. Mazur, and K. W. Hipps, “Structure, properties, and reactivity of porphyrins on surfaces and nanostructures with periodic DFT calculations,” *Appl. Sci.* **10**, 740 (2020).
- <sup>15</sup>M. Neamtu, C. Nadejde, L. Brinza, O. Dragos, D. Gherghel, and A. Paul, “Iron phthalocyanine-sensitized magnetic catalysts for BPA photodegradation,” *Sci. Rep.* **10**, 5376 (2020).
- <sup>16</sup>F. A. Nelson, H. Louis, I. Benjamin, and R. A. Timothy, “The iron group transition-metal (Fe, Ru, Os) coordination of se-doped graphitic carbon (Se@g-C<sub>3</sub>N<sub>4</sub>) nanostructures for the smart therapeutic delivery of zidovudine (ZVD) as an antiretroviral drug: A theoretical calculation perspective,” *RSC Adv.* **13**, 34078–34096 (2023).
- <sup>17</sup>N. A. Stephenson and A. T. Bell, “Mechanistic insights into iron porphyrin-catalyzed olefin epoxidation by hydrogen peroxide: Factors controlling activity and selectivity,” *J. Mol. Catal. A: Chem.* **275**, 54–62 (2007).